Control and Cybernetics
vol. **54** (2025) No. 1
pages: 49-77
DOI: 10.2478/candc-2025-0003

An integral feedback linearization applied to an aeropendulum*

by

Uiliam Nelson Lendzion Tomaz Alves[1*], Ricardo Breganon[1], Márcio Mendonça[2] and Rodrigo Henrique Cunha Palácios[2]

[1]Control and Industrial Processes, IFPR – Instituto Federal do Paraná, Av. Dr. Tito, 801, Jacarezinho, 86400-000, Paraná, Brazil
[2]Graduate Program in Mechanical Engineering (PPGEM-CP), UTFPR – Universidade Tecnológica Federal do Paraná, Av. Alberto Carazzai, 1640, Cornélio Procópio, 86300-000, Paraná, Brazil
*Corresponding author: uiliam.alves@ifpr.edu.br;
Contributing authors: ricardo.breganon@ifpr.edu.br; mendonca@utfpr.edu.br; rodrigopalacio@utfpr.edu.br

Abstract: Aeropendulum systems are nonlinear systems, in which a motor-propeller assembly drives a rod. They are used for educational purposes and testing control laws in real systems. Feedback linearization is a nonlinear control technique that algebraically linearizes a plant's dynamics via a feedback law and has been applied to various systems. This paper designs a feedback linearization control law incorporating an integrator into the control loop. The integrator enhances robustness in respect to constant disturbances, but alters the closed-loop dynamics, preventing it from following exactly the dynamics, associated with the desired characteristic roots under constant input. To address this, the integrator's initial condition is treated as an additional variable, selected to ensure the expected closed-loop response. Finally, simulations and bench experiments on an Aeropendulum system validate the approach, demonstrating the integrator's effectiveness in handling constant disturbances and the impact of selecting an appropriate initial condition.

Keywords: aeropendulum system, feedback linearization, integral control, tracking control

1. Introduction

The Aeropendulum system is a nonlinear system in which a rod is connected to a rotational axis. It is driven by a motor+propeller assembly at one end

*Submitted: March 2025; Accepted: August 2025.

of the rod, providing the necessary torque for the system's movement. The other end of the rod can contain a counterweight, so that the system requires less torque for the movement of the rod. The Aeropendulum can be used for teaching control techniques (Enikov and Campa, 2012; Breganon et al., 2021; Neto et al., 2023) or even for studying control strategies for nonlinear systems. In Saleem et al. (2020), it is observed that the Aeropendulum can be used in tests to validate control strategies for takeoff and landing of propeller-driven vehicles, such as multi-rotor drones, helicopters, rockets, balloons, harrier jets, etc.

Different control laws for Aeropendulum systems are found in the literature. For example, in Saleem et al. (2020), the authors study the use of an adaptive PID (Proportional–Integral–Derivative) control using fuzzy logic for an Aeropendulum system with two propellers. An identification method based on different operating points and a switched control law based on the model obtained by this method is presented in Silva et al. (2020). In Yamanaka et al. (2022), the authors present an Aeropendulum system where the control is performed using LQR (Linear Quadratic Regulator) with an integral control action. An Artificial Neural Network is used to control an Aeropendulum in Rafiuddin and Khan (2022), and an $\mathcal{H}_\infty$ control is used in Breganon et al. (2023).

Feedback linearization is a technique for controlling nonlinear systems that allows algebraically linearizing a system's dynamics through an adequate feedback control law. After this exact linearization, linear control techniques can be used to obtain the desired response from the closed-loop system, whether in regulation or tracking problems, see Slotine and Li (1991) or Khalil (2001). However, despite its versatility, classical feedback linearization may have difficulties controlling nonlinear systems with disturbances.

Feedback linearization strategies have been proposed in the literature to control different systems. In Mahmood and Kim (2017), feedback linearization is applied to the formation control of quadcopters, and then a sliding mode control is used to make the closed-loop system robust. Bagheri, Naseradinmousavi and Krstić (2019) formulated a predictor-based feedback linearization control for a robot manipulator, and Meng et al. (2022) proposed a feedback linearization control method by utilizing a nonlinear disturbance observer and applied it to a quadruple-tank liquid level system. A robust granular feedback linearization was presented in Oliveira et al. (2020a) and compared with Robust Multi-Inversion and Robust Dynamic Inversion techniques in Oliveira et al. (2020b), where tests were carried out in an actual surge tank in both works. In Chen, Yu and Chen (2020), feedback linearization and then robust control were used to deal with uncertainties in linear permanent magnet synchronous motors. The authors in Mehndiratta et al. (2020) have developed a Simple Learning strategy-based Feedback Linearization Control (SL-FLC) that is robust in the presence of uncertainties or disturbances and implemented it in a tilt-rotor tricopter unmanned aerial vehicle. Martins, Cardeira and Oliveira (2021) used feedback linearization with an integrator in the control loop and LQR for controlling a quadrotor.

This paper explores using an integrator in the linearization feedback loop to compensate for disturbances (Mehndiratta et al., 2020; Martins, Cardeira and Oliveira, 2021; Kayacan and Fossen, 2019; Csizmadia, Kuczmann and Orosz, 2022). The analysis and results show that this strategy makes the closed-loop system robust with respect to time-invariant disturbances. Furthermore, adding this integrator to the control loop modifies the system response, so that the response obtained differs from the response, specified in the design, through the desired characteristic roots for a constant input. The new degree of freedom, provided by the initial condition of the integrator and the methodology presented in Lu and Cheng (2005), which was extended to accommodate a generic number n of poles and allow for not necessarily repeated roots in the characteristic equation, are used to make the closed-loop system respond as expected. The results, obtained by simulation, and practical experiments with an Aeropendulum prototype, show the approach's effectiveness in a real system.

The main contributions of this paper can be summarized as follows. It introduces an integral feedback linearization control law for Aeropendulum systems, addresses the modification of closed-loop system dynamics, caused by the integrator, and analyzes the robustness against constant and derivative-bounded disturbances. The paper demonstrates how to select the integrator's initial condition as an additional variable in order to achieve the desired closed-loop system response for n-order systems with an integrator in the control loop. It validates the proposed approach through simulations and bench experiments on an Aeropendulum system and provides insights into using Aeropendulum systems as valuable tools for control law testing.

The rest of this paper is organized as follows. Section 2 reviews the theory of feedback linearization for a class of systems that includes the Aeropendulum dynamics. The use of the integrator, together with feedback linearization, is presented in Section 3. This section also analyzes the system's response with an integrator in the feedback loop and shows the initial condition calculation such that the system response corresponds to the desired behavior. In addition, it examines the closed-loop system performance under the influence of external disturbances. Section 4 describes the Aeropendulum system, its mathematical model, and the prototype used in the tests. The results obtained are shown in Section 5, and Section 6 concludes the study.

Notation: the argument t is omitted throughout the text for simplicity when this is convenient. A dot (two or three dots) above a variable denotes the time derivative (second or third time derivatives) of that variable. We use $x^{(n)}$ for representing the time derivatives of x of order higher than three, where n is the order of the derivative. $\mathcal{L}\{x\}$ denotes the Laplace Transform of x. $\Re\{p\}$ denotes the real part of the number p.

2. Feedback linearization

Consider a nonlinear system, described by

$$x^{(n)} = f(\chi) + b(\chi)u, \tag{1}$$

where $x \in \Re$ is the system's output, $f(\chi)$ and $b(\chi)$ are nonlinear functions, and $\chi = \begin{bmatrix} x & \dot{x} & \cdots & x^{(n-1)} \end{bmatrix}$.

Let the origin of the state space $x = \dot{x} = x^{(n-1)} = 0$ be the equilibrium point of the system (1). A feedback linearization control law for the system (1) is given by

$$u = \frac{1}{b(\chi)} \left(-f(\chi) + v\right) \tag{2a}$$

$$v = \alpha_0 e + \alpha_1 \dot{e} + \cdots + \alpha_{n-1} e^{(n-1)} + r^{(n)}, \tag{2b}$$

where

$$e = r - x \tag{3}$$

is the tracking error between the desired reference r with respect to the system's output x. It is assumed that $b(\chi) \neq 0$ during system operation.

Substituting (2) into (1) leads to

$$\begin{aligned} x^{(n)} &= f(\chi) + b(\chi)\left(\frac{1}{b(\chi)}\left(-f(\chi) + v\right)\right) \\ &= \alpha_0 e + \alpha_1 \dot{e} + \cdots + \alpha_{n-1} e^{(n-1)} + r^{(n)}. \end{aligned} \tag{4}$$

From (3), one deduces that $e^{(n)} = r^{(n)} - x^{(n)}$. Thus, (4) can be rewritten as

$$e^{(n)} + \alpha_{n-1} e^{(n-1)} + \cdots + \alpha_1 \dot{e} + \alpha_0 e = 0. \tag{5}$$

To ensure the stability of the tracking error and the convergence of x to r as t approaches infinity, the values of α_k, for $k = 0$ to $n-1$, must be selected such that the characteristic roots of (5) have real parts that are less than zero (see Slotine and Li, 1991; Khalil, 2001; or Lathi, 2005).

One way to find the parameters α_k in (5) is to choose suitable roots $-p_i$, for $i = 1$ to n (all of them with their real part less than zero) and compare the desired characteristic equation

$$\begin{aligned} Q(s) &= \prod_{i=1}^{n}(s+p_i) = (s+p_1)(s+p_2)\cdots(s+p_n) \\ &= s^n + \alpha_{n-1}s^{n-1} + \alpha_{n-2}s^{n-2} + \cdots + \alpha_1 s + \alpha_0 \end{aligned} \tag{6}$$

where

$$\alpha_k = \sum_{1 \le j_1 < j_2 < \cdots < j_{n-k} \le n} p_{j_1} p_{j_2} \cdots p_{j_{n-k}} \tag{7}$$

with (5). More details about feedback linearization can be found in Slotine and Li (1991) and Khalil (2001).

Example 1 *Let $n = 2$, then, from* (6),

$$Q(s) = s^2 + \alpha_1 s + \alpha_0$$

and we have two coefficients to determine. For $k = 1$, from (7)*, we have $j_{n-k} = j_{2-1} = j_1$ and*

$$\alpha_1 = \sum_{1 \le j_1 \le 2} p_{j_1} = p_1 + p_2. \tag{8}$$

For $k = 0$, $j_{n-k} = j_{2-0} = j_2$, and

$$\alpha_0 = \sum_{1 \le j_1 < j_2 \le 2} p_{j_1} p_{j_2} = p_1 p_2. \tag{9}$$

Example 2 *Let $n = 3$, from* (6) *it follows that*

$$Q(s) = s^3 + \alpha_2 s^2 + \alpha_1 s + \alpha_0$$

and we have three coefficients to determine. For $k = 2$, from (7)*, we have $j_{n-k} = j_{3-2} = j_1$ and*

$$\alpha_2 = \sum_{1 \le j_1 \le 3} p_{j_1} = p_1 + p_2 + p_3. \tag{10}$$

For $k = 1$, $j_{n-k} = j_{3-1} = j_2$ and

$$\alpha_1 = \sum_{1 \le j_1 < j_2 \le 3} p_{j_1} p_{j_2} = p_1 p_2 + p_1 p_3 + p_2 p_3. \tag{11}$$

Finally, for $k = 0$, $j_{n-k} = j_{3-0} = j_3$ and

$$\alpha_0 = \sum_{1 \le j_1 < j_2 < j_3 \le 3} p_{j_1} p_{j_2} p_{j_3} = p_1 p_2 p_3. \tag{12}$$

The primary advantage of the control law (2) is that it leads to linear closed-loop dynamics (5). Thus, it allows for the direct application of linear control synthesis techniques to achieve desired transient and steady-state performance. However, a significant limitation of this approach is its inherent sensitivity to parametric uncertainties, unmodeled nonlinear dynamics, and external disturbances. The linearization is exact only under the perfect knowledge of the plant dynamics (i.e., exact models of $f(\chi)$ and $b(\chi)$). Deviations, due to modeling errors or disturbances, disrupt the linear equivalence, potentially leading to tracking errors and/or performance loss.

To address these robustness limitations, Section 3 introduces an integral term within the feedback linearization framework that enhances the closed-loop system's rejection of constant disturbances and matched uncertainties.

3. Integral feedback linearization

3.1. Preliminaries

Uncertainties in parameter values and disturbances can change the equilibrium point of a system. When this occurs, integral control can help to regulate the error to zero (see Khalil, 2001; Mehndiratta et al., 2020; Kayacan and Fossen, 2019). In this subsection, an integrator is added to the control loop to address disturbances in plant dynamics. The inclusion of this additional integrator introduces a new state variable into the dynamics of the closed-loop system. This new state variable is expressed as follows

$$z(t) = \int_{\tau=0}^{t} e(\tau)d\tau + z(0), \tag{13}$$

where e is given in (3). Therefore, from (13), (3), and (1), one has

$$\begin{aligned}
\dot{z} &= e = r - x && \text{(14a)}\\
\ddot{z} &= \dot{e} = \dot{r} - \dot{x} && \text{(14b)}\\
&\vdots \\
z^{(n+1)} &= e^{(n)} = r^{(n)} - x^{(n)} = r^{(n)} - f(\chi) - b(\chi)u. && \text{(14c)}
\end{aligned}$$

Note that (14) has one state variable more than the original plant (1). The control law (2) can be easily modified for the new dynamics (14), becoming

$$u(t) = \frac{1}{b(\chi)}\left(-f(\chi) + v\right) \tag{15a}$$

$$v = \beta_0 z + \beta_1 \dot{z} + \cdots + \beta_n z^{(n)} + r^{(n)}. \tag{15b}$$

Substituting (15) into (14) results in

$$z^{(n+1)} + \beta_n z^{(n)} + \ \cdots \ + \beta_1 \dot{z} + \beta_0 z = 0. \tag{16}$$

For asymptotic convergence of the output x to the reference r, the parameters β_k, for $k = 0$ to n, must be selected so as to place all characteristic roots of (16) in the open left-half plane. Upon assigning the desired roots as $-p_i$, for $i = 0$ to $n+1$, the characteristic polynomial becomes

$$\begin{aligned} P_1(s) &= \prod_{i=1}^{n+1} (s + p_i) = (s + p_1)(s + p_2) \cdots (s + p_{n+1}) \\ &= s^{n+1} + \beta_n s^n + \beta_{n-1} s^{n-1} + \cdots + \beta_1 s + \beta_0, \end{aligned} \tag{17}$$

where the parameters β_k are

$$\beta_k = \sum_{1 \le j_1 < j_2 < \cdots < j_{(n+1)-k} \le (n+1)} p_{j_1} p_{j_2} \cdots p_{j_{(n+1)-k}}. \tag{18}$$

3.2. Disturbance analysis

The presence of disturbances in the system dynamics (1), along with the integral feedback linearization control (15), is now analyzed. Consider a disturbance in the plant dynamics, such that it can be described as

$$x^{(n)} = f(\chi) + b(\chi)u + d, \tag{19}$$

where d represents matched disturbances. Using (19) and the control law (15), the dynamics (16) becomes (Mehndiratta et al., 2020; Kayacan and Fossen, 2019)

$$z^{(n+1)} + \beta_n z^{(n)} + \ \cdots \ + \beta_1 \dot{z} + \beta_0 z = d. \tag{20}$$

Taking into account (13) and (14), from (20), one has

$$e^{(n)} + \beta_n e^{(n-1)} + \cdots + \beta_1 e + \beta_0 \left[\int_{\tau=0}^{t} e(\tau) d\tau + z(0) \right] = d, \tag{21}$$

which yields (Mehndiratta et al., 2020; Kayacan and Fossen, 2019)

$$e^{(n+1)} + \beta_n e^{(n)} + \cdots + \beta_1 \dot{e} + \beta_0 e = \dot{d}. \tag{22}$$

Since the roots of the characteristic equation (17) have real parts less than zero, if d is such that $\dot{d} = 0$, the error in (22) converges to zero (Lathi, 2005), even in the presence of disturbances.

Consider a non-constant disturbance $d(t)$, such that

$$\left|\dot{d}(t)\right| \leq D. \tag{23}$$

The closed-loop system (22) is linear, and so its response can be described as (Lathi, 2005)

$$e(t) = e_0(t) + e_u(t), \tag{24}$$

where $e_0(t)$ is zero-input response and $e_u(t)$ is zero-state response. Then, $e_0(t)$ is a combination of the characteristic modes of the system. In this case, by choosing β_k as in (18), $-p_k < 0$, we can find (Lathi, 2005)

$$e_0(t) = \sum_{k=1}^{n+1} c_k e^{-p_k t} \cdot m_k(t) \leq q e^{-p_{\max} t}, \tag{25}$$

$$-p_{\max} = \max_i \{\Re\{-p_i\}\} < 0, \tag{26}$$

where c_k, for $k = 1$ to $n+1$, are constants that depend on the initial conditions of the system and $m_k(t)$ are polynomials of t, when the characteristic roots of (17) are repeated. Further, $q > 0$ is a constant that depends on the values of c_k. It is important to note that, when choosing the real part of $-p_k$ less than zero, $e_0(t) \to 0$ when $t \to \infty$.

The zero-state response $e_u(t)$ is due to the external input $\dot{d}(t)$ and is computed via convolution with the system's impulse response (Lathi, 2005),

$$e_u(t) = \int_{\tau=0}^{t} \dot{d}(t-\tau) h(\tau) d\tau, \tag{27}$$

where $h(t)$ represents the impulse response of the linear dynamics (22). Then,

$$\begin{aligned} |e_u(t)| &= \left| \int_{\tau=0}^{t} \dot{d}(t-\tau) h(\tau) d\tau \right| \\ &\leq \int_{\tau=0}^{t} \left| \dot{d}(t-\tau) h(\tau) \right| d\tau \\ &= \int_{\tau=0}^{t} \left| \dot{d}(t-\tau) \right| |h(\tau)| \, d\tau. \end{aligned} \tag{28}$$

Given the bounded disturbance derivative $|\dot{d}(t)| \leq D$, equation (23), the magnitude of $e_u(t)$ in (28) satisfies

$$|e_u(t)| \leq D \int_{\tau=0}^{t} |h(\tau)| \, d\tau. \tag{29}$$

The impulse response $h(t)$ can be calculated from the transfer function of (22). Then, taking into account (17), we have

$$\begin{aligned} H(s) &= \frac{\mathcal{L}\{e(t)\}}{\mathcal{L}\{\dot{d}(t)\}} = \frac{1}{P_1(s)} \\ &= \frac{1}{\prod_{i=1}^{n+1}(s+p_i)}. \end{aligned} \tag{30}$$

The inverse Laplace transform of (30) yields

$$h(t) = \sum_{k=1}^{n+1} g_k e^{-p_k t} \cdot m_k(t) \leq \hat{q} e^{-p_{\max} t}, \tag{31}$$

where g_k, for $k = 1$ to $n+1$, are coefficients to be determined, based on the energy that the impulse input provides to the system, $m_k(t)$ denotes the polynomial terms for repeated roots, $\hat{q} > 0$ is a constant that depends on g_k, and $-p_{\max}$ is given in (26). Since all poles $-p_k$ have negative real parts, the envelope of $|h(t)|$ decays exponentially. We can write

$$|h(t)| \leq \hat{q} e^{-p_{\max} t}. \tag{32}$$

From (29) and (32), it follows that

$$\begin{aligned} |e_u(t)| &\leq D\hat{q} \int_{\tau=0}^{t} e^{-p_{\max}\tau} d\tau \\ &= D\hat{q} \left(\frac{e^{-p_{\max}\tau}}{-p_{\max}} \bigg|_{\tau=0}^{t} \right) \\ &= D\hat{q} \left(\frac{e^{-p_{\max}t} - 1}{-p_{\max}} \right). \end{aligned} \tag{33}$$

Let $t \to \infty$, because $-p_{\max} < 0$, from (33) one can find that

$$\lim_{t \to 0} |e_u(t)| \leq \frac{D\hat{q}}{p_{\max}} > 0. \tag{34}$$

Finally, from (24), (25) and (34)

$$\begin{aligned} \lim_{t \to 0} |e(t)| = \lim_{t \to 0} |e_0(t) + e_u(t)| &\leq \lim_{t \to 0} (|e_0(t)| + |e_u(t)|) \\ &\leq 0 + \frac{D\hat{q}}{p_{\max}} = \frac{D\hat{q}}{p_{\max}}. \end{aligned} \tag{35}$$

Equation (35) shows that the error $e(t) = y(t) - r(t)$ is bounded for the closed-loop system when the disturbance has its derivative also bounded.

3.3. Integrator's initial condition

Upon including an integrator in the feedback loop, the order of the system is increased. The new state variable is given by (13). The value of $z(0) = e(0)$ is the degree of freedom that can be adequately selected to obtain the desired response (Lu and Cheng, 2005).

The idea is to choose the initial condition in (13) such that the closed-loop system (1) and (15) exhibits the desired characteristics. To achieve this, the methodology presented in Lu and Cheng (2005) is extended to select the initial condition, considering a system of order n and different characteristic roots.

Let the poles $-p_i < 0$, for $i = 1$ to $n+1$ be given, such that the relationship between the reference for the system $R(s)$ and the system's output $X(s)$, the transfer function of the system, is such that

$$\frac{X(s)}{R(s)} = \frac{\beta_0}{P_1(s)} = \frac{\prod_{i=1}^{n+1} p_i}{\prod_{i=1}^{n+1}(s+p_i)}, \tag{36}$$

where $P_1(s)$ is given in (17), and the coefficients β_k are given by (18).

For a constant reference input r and zero initial conditions, from (36), the output $X(s)$ is calculated as

$$X(s) = \frac{\beta_0}{P_1(s)}\frac{r}{s} = \frac{r\prod_{i=1}^{n+1} p_i}{s\prod_{i=1}^{n+1}(s+p_i)}. \tag{37}$$

We now analyze the response of the closed-loop system to a constant input r. The dynamics is based on (16), so that

$$z^{(n+1)} + \beta_n z^{(n)} + \cdots + \beta_1 \dot{z} + \beta_0 z = r. \tag{38}$$

Aplying the Laplace transform in (38), we arrive at

$$\mathcal{L}\{z^{(n+1)}\} + \beta_n \mathcal{L}\{z^{(n)}\} + \cdots + \beta_1 \mathcal{L}\{\dot{z}\} + \beta_0 \mathcal{L}\{z\} = \mathcal{L}\{r\}. \tag{39}$$

The time differentiation property gives us (Lathi, 2005):

$$\mathcal{L}\left\{\frac{d^n z(t)}{dt^n}\right\} = s^n Z(s) - \sum_{k=1}^{n} s^{n-k} z^{(k-1)}(0). \tag{40}$$

Then, from (40), we have

$$\begin{aligned}\mathcal{L}\{z^{(n+1)}(t)\} &= s^{n+1}Z(s) - s^{n}z(0) - s^{(n-1)}\dot{z}(0)\\ &\quad - s^{(n-2)}\ddot{z}(0) - \cdots - sz^{(n-1)}(0) - z^{(n)}(0) \qquad (41a)\\ \mathcal{L}\{z^{(n)}(t)\} &= s^{n}Z(s) - s^{n-1}z(0) - s^{(n-2)}\dot{z}(0)\\ &\quad - \cdots - sz^{(n-2)}(0) - z^{(n-1)}(0) \qquad (41b)\\ &\ \ \vdots\\ \mathcal{L}\{\ddot{z}(t)\} &= s^{2}Z(s) - sz(0) - \dot{z}(0) \qquad (41c)\\ \mathcal{L}\{\dot{z}(t)\} &= sZ(s) - z(0) \qquad (41d)\\ \mathcal{L}\{z(t)\} &= Z(s). \qquad (41e)\end{aligned}$$

Given that r is constant, based on the definition (14), the initial conditions for (38) are $z(0)$, and

$$\dot{z}(0) = e(0) = r - x(0) = r \qquad (42a)$$

$$z^{(n)}(0) = e^{(n-1)}(0) = -x^{(n-1)}(0) = 0,\ n \geq 2. \qquad (42b)$$

The closed-loop dynamics (38) in the Laplace domain incorporate initial conditions via the differentiation property (40). Then, from (39), (41), and (42), we have

$$\begin{aligned}&\left(s^{n+1}Z(s) - s^{n}z(0) - s^{n-1}r\right)\\ &+\beta_n\left(s^{n}Z(s) - s^{n-1}z(0) - s^{n-2}r\right)\\ &+\ \cdots + \beta_2\left(s^{2}Z(s) - sz(0) - r\right)\\ &+\beta_1\left(sZ(s) - z(0)\right) + \beta_0 Z(s) = r/s,\end{aligned}$$

which can be rewritten as

$$\begin{aligned}&Z(s)\left(s^{n+1} + \beta_n s^{n} + \cdots + \beta_2 s^2 + \beta_1 s + \beta_0\right)\\ &-z(0)\left(s^{n} + \beta_n s^{n-1} + \cdots + \beta_2 s + \beta_1\right)\\ &-r\left(s^{n-1} + \beta_n s^{n-2} + \cdots + \beta_3 s + \beta_2\right) = r/s. \qquad (43)\end{aligned}$$

Using $P_1(s)$, defined in (17), and defining

$$P_2(s) = s^{n} + \beta_n s^{n-1} + \cdots + \beta_2 s + \beta_1 \qquad (44)$$

$$P_3(s) = s^{n-1} + \beta_n s^{n-2} + \cdots + \beta_3 s + \beta_2, \qquad (45)$$

equation (3.3) can be rewritten as

$$\begin{aligned}&Z(s)P_1(s) - z(0)P_2(s) - rP_3(s) = r/s\\ &Z(s) = \frac{z(0)P_2(s) + rP_3(s) + r/s}{P_1(s)}. \qquad (46)\end{aligned}$$

From (14a), we have that $x = r - \dot{z}(t)$, which, using Laplace transform, becomes

$$X(s) = \mathcal{L}\{r(t)\} - \mathcal{L}\{\dot{z}(t)\} = r/s - (sZ(s) - z(0))\,. \tag{47}$$

From (37), (46) and (47)

$$\frac{\beta_0 r}{sP_1(s)} = \frac{r}{s} - \frac{s[z(0)P_2(s) + rP_3(s)] + r}{P_1(s)} + z(0)$$

$$\beta_0 r = rP_1(s) - s^2[z(0)P_2(s) + rP_3(s)] - rs + sz(0)P_1(s). \tag{48}$$

By the definitions in (17), (44), and (45), we have

$$P_2(s) = sP_3(s) + \beta_1 \tag{49}$$
$$P_1(s) = sP_2(s) + \beta_0 = s^2P_3(s) + \beta_1 s + \beta_0. \tag{50}$$

Using (49) and (50), (48) can be rewritten as

$$\begin{aligned}
\beta_0 r &= r\left(s^2P_3(s) + \beta_1 s + \beta_0\right) \\
&\quad -s^2[z(0)\left(sP_3(s) + \beta_1\right) + rP_3(s)] - rs \\
&\quad +sz(0)\left(s^2P_3(s) + \beta_1 s + \beta_0\right) \\
&= rs^2P_3(s) + r\beta_1 s + r\beta_0 \\
&\quad -z(0)s^3P_3(s) - z(0)\beta_1 s^2 - rs^2P_3(s) - rs \\
&\quad +z(0)s^3P_3(s) + z(0)s^2\beta_1 + z(0)s\beta_0 \\
&= r\beta_1 s + r\beta_0 + z(0)s\beta_0 - rs.
\end{aligned} \tag{51}$$

Therefore, from (3.3),

$$r\beta_1 s + z(0)s\beta_0 - rs = 0.$$

Finally, one can find

$$z(0) = \frac{r}{\beta_0} - \frac{r\beta_1}{\beta_0} = \frac{r(1-\beta_1)}{\beta_0}. \tag{52}$$

Using the initial condition (52) in (13), the behavior specified in the characteristic equation (16), the denominator of the transfer function (36), is achieved for the closed-loop system (1) and (15).

Similarly, when the system is subjected to a constant disturbance, the right hand side of equation (38) becomes $r+d$, and we calculate the initial condition for the integrator as

$$z(0) = \frac{r+d}{\beta_0} - \frac{r\beta_1}{\beta_0}. \tag{53}$$

One can observe that the value of the disturbance d is not known, so the designer should employ some strategy to estimate its value. Future research may focus on automating the selection of the integrator's initial condition, when the system is subjected to disturbances, thereby enhancing the applicability of the proposed approach in practical scenarios.

The use of an integral action within the feedback linearization framework significantly enhances the robustness to constant disturbances by systematically eliminating steady-state errors, as shown in Subsection 3.2. However, this method introduces two key limitations: (i) dependence on reasonably accurate parameter estimates to preserve the linearized model's structure, and (ii) sensitivity to the integrator's initial condition $z(0)$, which dictates transient performance. In practical implementations, determining $z(0)$ may necessitate additional estimation or calibration steps. Despite these challenges, the results in Section 5 demonstrate the method's efficacy through simulations and experimental tests on an Aeropendulum system, validating its utility for real-world applications.

4. Aeropendulum system

4.1. The description

Figure 1 shows a schematic sketch of an Aeropendulum system. This system consists of a rod fixed to a rotational axis A_r. A motor+propeller assembly is coupled to this rod at one of its ends; at the other end, there is a counterweight. In this schematic sketch the center of mass of the rod+motor+propeller assembly is denoted by c_{m1}, and the center of mass of the counterweight is indicated by c_{m2}. L_1 is the distance between A_r and c_{m1}. L_2 is the distance between A_r and c_{m2}. The angle between the rod and its rest position is given by θ and represents the system's output. The torque τ, which is the system's input, moves the rod.

The dynamics of the Aeropendulum system can be described using Newton's second law of rotation (Enikov and Campa, 2012; Lucena, Luiz and Lima, 2021). By putting together the sum of torques on the rotational axis, from Fig. 1, one finds

$$\tau - m_1 g L_1 \sin(\theta) + m_2 g L_2 \sin(\theta) - b\dot{\theta} = I\ddot{\theta}, \tag{54}$$

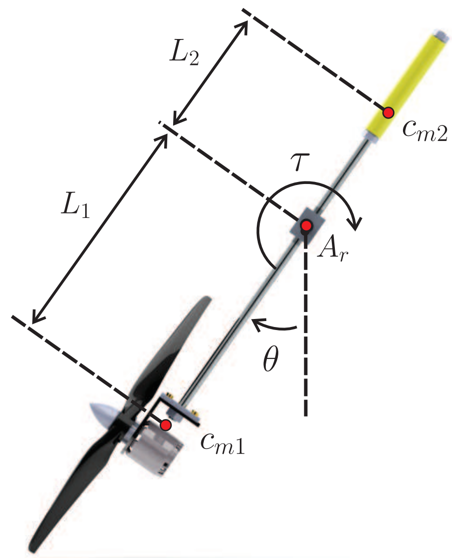

Figure 1. Schematic sketch of an Aeropendulum system (adapted from Yamanaka et al., 2022)

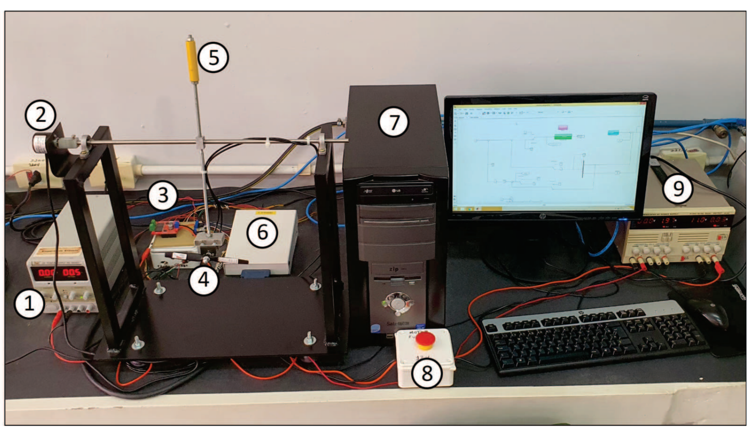

Figure 2. Aeropendulum prototype present in the Automation and Control laboratory of the IFPR campus Jacarezinho (adapted from Yamanaka et al., 2022)

where τ [N.m] is the torque, produced by the motor+propeller assembly, m_1 [kg] is the mass of the rod+motor+propeller assembly, L_1 [m] is the distance from the center of mass of the rod+motor+propeller assembly to the rotational axis, m_2 [kg], the total mass of the counterweight, L_2 [m], the distance from the center of mass of the counterweight to the rotational axis, I [N.m^2], the total moment of inertia, b [N.m.s/rad], the coefficient of viscous friction, g [m/s^2], the acceleration of gravity. Finally, θ [rad] represents the angle of the rod with respect to the resting position.

Note that (54) can be represented by the model (1), where $\chi = \begin{bmatrix}\theta & \dot{\theta}\end{bmatrix}$, $u = \tau$,

$$f(\chi) = \frac{-m_1 g L_1 \sin(\theta) + m_2 g L_2 \sin(\theta) - b\dot{\theta}}{I}, \tag{55a}$$

$$b(\chi) = \frac{1}{I}. \tag{55b}$$

4.2. Aeropendulum prototype

The Aeropendulum prototype, present in the IFPR campus Jacarezinho, is shown in Fig. 2 (see Yamanaka et al., 2022) in which numbers identify the prototype's components. The 5 V source ① energizes the incremental rotational encoder LPD 3806-600BM-G5-24C, with 600 PPR (Pulses Per Revolution) ②. This encoder measures the rod's angular position during the Aeropendulum's operation. A PWM (Pulse Width Modulation) signal drives the propulsion set, composed of a 12 V Direct Current (DC) motor, with power of 4.85 W, 53 gf.cm of torque, and a nominal speed of 12500 rpm. A Monster Motor Shield VNH3ASP30 H-bridge with a 30 A current capacity ③ converts the PWM signal into voltage to drive the motor. The DC motor allows the 6" x 3.5 ④ propeller to generate the thrust force, responsible for performing the angular movement of the rod. A counterweight is installed to reduce the thrust force, required for the movement, and it is indicated by ⑤.

In Fig. 2, the H-bridge and the encoder are connected to a data acquisition board from National Instruments®, model PCI-6602, through a connector block ⑥. This acquisition board is responsible for reading the rod angle, providing this information to the control software, and sending the calculated PWM signal to the H-bridge. It allows reading the encoders through quadrature, increasing its resolution by four times. An Intel Core 2 Duo E8600 3.33 GHz computer ⑦, with 2 GB of RAM, controls the system using the Matlab/Simulink® software. In addition, an emergency stop button has been installed to ensure safe operation in case of unexpected system behavior ⑧. Finally, a 12 V DC source ⑨ drives the motor through the H-bridge. By using this setup, it is possible to implement the controller with a sampling period of $T_s = 0.02$ s, which was used in the experiments, and the Matlab/Simulink® guarantees the real-time implementation of the control law.

The parameters of the Aeropendulum prototype, shown in Fig. 2, are presented in Table 1. The viscous friction coefficient of the rotational axis was obtained from the free-swinging movement of the rod in a similar manner as obtained by Breganon et al. (2021b). The moments of inertia I was calculated by summing the moment of inertia of each element that composes the equipment around A_r in Fig. 1. It was considered to consist of the moment of inertia of the rod of the pendulum and of the rod of the counterweight, the motor+propeller assembly, and the counterweight.

Table 1. Parameters of the Aeropendulum prototype shown in Fig. 2

Parameter	**Symbol**	**Value [unit]**
Gravity acceleration	g	9.81 [m/s^2]
Rod+motor+propeller mass	m_1	0.1183 [kg]
Distance from the rotational axis to the center of mass of the rod+motor+propeller assembly	L_1	0.2019 [m]
Mass of the counterweight	m_2	0.1086 [kg]
Distance from the rotational axis to the center of mass of the counterweight	L_2	0.0855 [m]
Viscous friction coefficient on the rotational axis	b	0.0098 [N.m.s/rad]
Total moment of inertia of the system	I	0.0065 [N.m^2]

The Aeropendulum model (54) has the torque from the thrust, generated by the motor+propeller assembly, as the control input. However, the signal for activating the prototype is sent to the H-bridge in PWM. Thus, it is necessary to convert the torque, calculated by the controller, into a PWM signal before sending it to the H-bridge.

As pointed out by Lucena, Luiz and Lima (2021), the dynamics between the PWM and the torque, generated by the motor+propeller, can be disregarded, because it is much faster than the mechanical response of the Aeropendulum dynamics. So, it was considered that a simple polynomial function represents the torque conversion to PWM. Tests were carried out on the prototype to map the PWM and torque relation. A PWM signal was sent to the system, and then the encoder measured the resulting angle after the system reached equilibrium.

Since, by the condition (54), for $\ddot{\theta} = \dot{\theta} = 0$, one has (Enikov and Campa, 2012; Lucena, Luiz and Lima, 2021)

$$\tau = m_1 g L_1 \sin(\theta) - m_2 g L_2 \sin(\theta), \tag{56}$$

and the torque, generated by the motor+propeller assembly, can be calculated by (56) from the measured angle θ.

The torque and PWM values, measured in the tests with the prototype, were

$$\begin{aligned} \mathrm{PWM} &= [0\ \ 0.1\ \ 0.2\ \ 0.3\ \ 0.4\ \ 0.5\ \ 0.6\ \ 0.7] \\ \tau &= [0\ \ 0\ \ 0.0112\ \ 0.0257\ \ 0.0460\ \ 0.0620\ \ 0.0916\ \ 0.1242]. \end{aligned} \tag{57}$$

With the test results, the torque×PWM relationship was approximated by a polynomial of degree 3. The polynomial found was

$$\mathrm{PWM}(\tau) = 328.3835\tau^3 - 90.9502\tau^2 + 11.4195\tau + 0.0579. \tag{58}$$

The measured data (57) and the values calculated with the aid of the polynomial (58) are shown in Fig. 3.

Therefore, in the control of the prototype, the control signal in the torque, given by the controller, is converted into a PWM using the polynomial (58) and then sent to drive the prototype's motor+propeller through the H-bridge.

5. Results and discussion

5.1. The setup

This section presents the tests carried out and the results obtained. First, the use of feedback linearization in the Aeropendulum system was studied both through simulation and through experiments with the prototype. Despite the fact, that there is no steady-state error in the simulation, the disturbances/uncertainties in the model caused a steady-state error during implementation using feedback linearization without an integrator in the control loop. After that, simulations using integral feedback linearization demonstrate the importance of choosing the integrator's initial condition, because it influences the closed-loop system's response. Finally, satisfactory simulation and implementation results of the integral feedback linearization were obtained for the use of the adequate choice of the initial state.

To ensure the desired closed-loop behavior, we selected the controller poles based on a combination of simulations and experimental tests with the prototype. It is worth noting that all poles must lie in the open left half of the complex

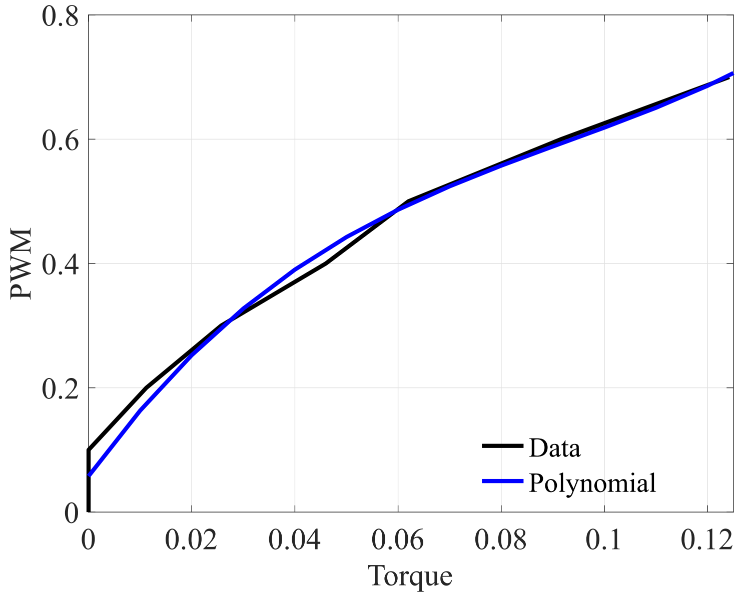

Figure 3. PWM as a function of torque for the Aeropendulum prototype, shown in Fig. 2

plane (i.e., have negative real parts) to guarantee system stability. The data obtained in the experiments with the prototype and simulations are available in Alves (2025).

5.2. Feedback linearization

The roots chosen for the linear dynamics (5) were $-p_1 = -3.5$ and $-p_2 = -6$. From Example 1, equations (9) and (8), one has $\alpha_1 = 9.5$, and $\alpha_0 = 21$. Thus, the control law (2), considering (55), becomes

$$u = m_1 g L_1 \sin(\theta) - m_2 g L_2 \sin(\theta) + b\dot{\theta} + I\left(\alpha_0 e + \alpha_1 \dot{e} + \ddot{r}\right). \quad (59)$$

Figure 4 presents the results from simulation and practical implementation in the prototype, described in Subsection 4.2, with the control law (59). It was assumed that there were zero initial conditions for the system, and a step-like reference, described by

$$
r_s(t) = \begin{cases} 0 \text{ rad}, & 0 \leqslant t < 20 \text{ s}, \\ 0.2618 \text{ rad}, & 20 \leqslant t < 40 \text{ s}, \\ 0.5236 \text{ rad}, & 40 \leqslant t < 60 \text{ s}, \\ 0.7854 \text{ rad}, & 60 \leqslant t < 80 \text{ s}. \end{cases} \tag{60}
$$

In order to reduce spikes or even control input saturation when using the reference (60), it was considered that $\dot{r}_s(t) = 0$ for calculating the control signal during simulation and experiments.

Table 2 presents the reference value, steady-state position, settling time, and steady-state error in % after each step in (60), obtained from both simulated and experimental responses for the results shown in Fig. 4 at the end of the paper. Each reference value is evaluated over a specific time interval, and results are shown separately for the simulated and experimental cases. The steady-state error is only reported for the experimental data. The settling time, defined as the time for the response to reach and stay within 2% of its final value, Nise (2019), was longer during the experiment in the first and second steps because the system took longer to achieve equilibrium.

Table 2. Simulated and experimental values of position, settling time, and steady-state error for the control law (59) controlling the Aeropendulum system

Ref. [rad]	**Type**	**Steady-state [rad]**	**Settling time [s]**	**Steady-state error [%]**
0.2618	Sim.	0.2618	21.36	0
	Exp.	0.1361	32.82	48.01
0.5236	Sim.	0.5236	41.16	0
	Exp.	0.3665	51.52	30.00
0.7854	Sim.	0.7854	61.04	0
	Exp.	0.5943	61.56	24.33

From the data, presented in Fig. 4 and Table 2, one can observe that despite adequate performance during the simulation, there was a steady-state error in the practical implementation.

5.3. Integral feedback linearization

The characteristic roots $-p_1 = -2$, $-p_2 = -3$ and $-p_3 = -8$ were chosen to design the integral feedback linearization. Thus, using (18), one has $\beta_0 = 48$,

$\beta_1 = 46$ and $\beta_2 = 13$ (see Example 2 and equations (10), (11), and (12) for details). Therefore, the control law (15), considering (55), becomes

$$u(t) = -m_1 g L_1 \sin(\theta) + m_2 g L_2 \sin(\theta) - b\dot{\theta} + I\left(\beta_0 z + \beta_1 \dot{z} + \beta_2 \ddot{z} + \dddot{r}\right). \tag{61}$$

To calculate the initial condition for the integrator, we used (52).

Figure 5, also at the end of the paper, presents the simulation results of the Aeropendulum system using the initial condition $z(0) = 0$ and $z(0)$, given by (52), and the control law (61). As it is possible to observe, the system's output presents an overshoot when the initial condition is chosen as zero, an undesirable fact with the choice of real roots for the error dynamics. For step 1, the peak value was 0.3115, resulting in an overshoot of 18.98%; for step 2, the peak was 0.5761 with an overshoot of 10.03%; and for step 3, the peak was 0.8387, corresponding to 6.79% overshoot. Additionally, the control signal exhibits a sharp initial pulse when the initial condition is set to zero, which may lead to actuator saturation or wear. Overshoot was removed with the proper choice of the initial condition. Note that, with the initial condition, the result of the controlled system and the desired transfer function (36) are identical.

The curves in Fig. 6 show the results, obtained from an experiment carried out with the Aeropendulum prototype in closed-loop with integral feedback linearization (61) using reference (60). Contrary to what is shown in Fig. 4, the error tends to zero even in the presence of disturbances. Note that the control signal, calculated in the experiment with the prototype, is greater than that calculated in the simulation. This fact evidences that the integral action of the control compensates for disturbances present in the prototype.

Table 3 shows the steady-state position, settling time, and overshoot obtained from simulated and experimental responses for the reference (60). The overshoot is reported in both absolute value and percentage and is only observed in the experimental results. The table highlights the system's transient behavior under different operating conditions. Although the experimental results showed an overshoot, these values are less than 7%. As presented in equation (53), to exactly obtain the initial condition that leads to no overshoot, it would be necessary to know or estimate the disturbance. In this experiment, the simulated and experimental values of settling time were found to be similar.

Finally, Fig. 7 shows the result of the closed-loop system with integral feedback linearization (61) using reference (62), where $\omega = 2\pi 40$ rad/s and $A = 0.2618$ rad. In this case, the control law (61) needs the first and second derivatives of the reference, which are given in (63) and (64), respectively. It is observed that the system maintained a good performance, following the reference, even when the reference changes over time. Again, the integral action

Table 3. Simulated and experimental values of position, settling time, and overshoot for the control law (61) controlling the Aeropendulum system

Ref. [rad]	**Type**	**Steady-state [rad]**	**Settling time [s]**	**Overshoot**	
				Value [rad]	**[%]**
0.2618	Sim.	0.2618	22.59	0	0
	Exp.	0.2618	22.64	0.2801	6.99
0.5236	Sim.	0.5236	42.24	0	0
	Exp.	0.5236	43.60	0	0
0.7854	Sim.	0.7854	62.02	0	0
	Exp.	0.7854	63.40	0.8142	3.67

compensated for disturbances, present in the real prototype,

$$r_d(t) = \begin{cases} 0.2618 \text{ rad}, & 0 \leqslant t < 20 \text{ s}, \\ 0.5236 \text{ rad}, & 20 \leqslant t < 40 \text{ s}, \\ A\sin(\omega t) \text{ rad}, & 40 \leqslant t < 160 \text{ s}. \end{cases} \tag{62}$$

$$\dot{r}_d(t) = \begin{cases} 0 \text{ rad}, & 0 \leqslant t < 40 \text{ s}, \\ A\omega\cos(\omega t) \text{ rad/s}, & 40 \leqslant t < 160 \text{ s}. \end{cases} \tag{63}$$

$$\ddot{r}_d(t) = \begin{cases} 0 \text{ rad}, & 0 \leqslant t < 40 \text{ s}, \\ -A\omega^2\sin(\omega t) \text{ rad/s}^2, & 40 \leqslant t < 160 \text{ s}. \end{cases} \tag{64}$$

6. Conclusion

The work, reported in this paper, used feedback linearization with integral action to control an Aeropendulum system. Although feedback linearization without integral action presents a good performance in controlling this system in simulation, in the presence of disturbances, inherent to practical implementation, the system with this controller presented steady-state error. In this context, integral action was able to deal with the real plant and conduct to adequate tracking results. However, when the initial condition of the control loop integrator was zero, the system output presented an overshoot in the simulation for constant reference. This fact is not expected when the characteristic roots for the error dynamics are chosen with zero imaginary parts. Nevertheless, the convenient choice of the integrator's initial condition allowed the system to present performance consistent with the selected characteristic roots.

Using the integrator and the appropriate initial condition enabled good reference tracking in simulation and experimental tests with the Aeropendulum prototype. This proves to be an adequate technique to control nonlinear systems with constant uncertainties or disturbances. The class of systems represented by (1) is utilized in the controller design, presented in this paper. While this class of systems has significant applications in representing real plants, there is a need to expand it to MIMO nonlinear systems in future works.

It is worth noting that the proposed control strategy has shown promising results in terms of robustness with regard to constant disturbances and ease of implementation. A quantitative comparison with other control approaches, such as $\mathcal{H}_\infty$ or adaptive control techniques, has not been conducted in this work and is the object of future research.

Acknowledgments

The authors would like to thank the IFPR campus Jacarezinho and the UTFPR campus Cornélio Procópio for their support in the development of this work.

Data and Code Availability

The datasets generated and/or analyzed during the current study, as well as the Matlab/Simulink® models used for simulations and controller implementation, are publicly available in the Mendeley Data repository: https://data.mendeley.com/datasets/9vx366bfm3/2.

References

Alves, U.N.L.T. (2025) *An Integral Feedback Linearization Applied to an Aeropendulum – Models, Parameters, and Measurement Data*. Publisher: Mendeley Data. https://doi.org/10.17632/9vx366bfm3.2

Bagheri, M., Naseradinmousavi, P. and Krstić, M. (2019) Feedback linearization based predictor for time delay control of a high-dof robot manipulator. *Automatica* **108**, 108485 https://doi.org/10.1016/j.automatica.2019.06.037

Breganon, R., Alves, U.N.L.T., Almeida, J.P.L.S., Ribeiro, F.S.F., Mendonça, M., Palácios, R.H.C. and Montezuma, M.A.F. (2021) Loop-shaping $\mathcal{H}_\infty$ control of an aeropendulum model. *International Journal of Applied Mechanics and Engineering* **26**(4), 1–16 https://doi.org/10.2478/ ijame-2021-0046

Breganon, R., Alves, U.N.L.T., Ribeiro, F.S.F., Barbara, G.V., Almeida, J.P.L.S., Pivovar, L.E., Montezuma, M.A.F. and Mendonça, M. (2021a) Development of inverted pendulum systems as didactical tools in courses of control and automation engineering. *Holos* **5**, 1–14 https://doi. org/10.15628/holos.2021. 10351. In Portuguese.

Breganon, R., Alves, U.N.L.T., Almeida, J.P.L.S., Ribeiro, F.S.F., Mendon¸ca, M., Palácios, R.H.C. and Montezuma, M.A.F. (2023) Model identification and H control of an aeropendulum. *Journal of Applied Research and Technology* **21**(4), 526–534 https://doi. org/10.22201/icat.24486736e.2023.21.4.1741

Chen, Y.T., Yu, C.S. and Chen, P.N. (2020) Feedback linearization based robust control for linear permanent magnet synchronous motors. *Energies* **13** https://doi. org/10.3390/en13205242

Csizmadia, M., Kuczmann, M. and Orosz, T. (2022) A novel control scheme based on exact feedback linearization achieving robust constant voltage for boost converter. *Electronics* **12**, 57 https://doi.org/10.3390/electronics12010057

Enikov, E.T. and Campa, G. (2012) Mechatronic aeropendulum: Demonstration of linear and nonlinear feedback control principles with matlab/simulink real-time windows target. *IEEE Transactions on Education* **55**, 538–545 https://doi.org/10.1109/TE.2012. 2195496

Kayacan, E. and Fossen, T.I. (2019) Feedback linearization control for systems with mismatched uncertainties via disturbance observers. *Asian Journal of Control* **21**, 1064–1076 https://doi.org/10.1002/asjc.1802

Khalil, H.K. (2001) *Nonlinear Systems*, 3rd edn. Prentice Hall, Upper Saddle River, NJ.

Lathi, B.P. (2005) *Linear Systems and Signals*, 3rd edn. Oxford University Press, New York.

Lu, Y.-S. and Cheng, C.-M. (2005) Design of a non-overshooting pid controller with an integral sliding perturbation observer for motor positioning systems. *JSME International Journal Series C* **48**, 103–110 https://doi.org/10.1299/jsmec.48.103

Lucena, E.R., Luiz, S.O.D. and Lima, A.M.N. (2021) Modeling, parameter estimation, and control of an aero-pendulum. In: *Procedings do XV Simpósio Brasileiro de Automação Inteligente*. SBA Sociedade Brasileira de Automática, Rio Grande, Brazil, 1984–1989. https://doi.org/10.20906/sbai.v1i1.2837

Mahmood, A. and Kim, Y. (2017) Decentrailized formation flight control of quadcopters using robust feedback linearization. *Journal of the Franklin Institute* **354**, 852– 871 https://doi.org/10.1016/j.jfranklin.2016. 10.039

Martins, L., Cardeira, C. and Oliveira, P. (2021) Feedback linearization with zero dynamics stabilization for quadrotor control. *Journal of Intelligent and Robotic Systems* **101**, 7 https://doi.org/10.1007/ s10846-020-01265-2

Meng, X., Yu, H., Zhang, J., Xu, T., Wu, H. and Yan, K. (2022) Disturbance observer-based feedback linearization control for a quadruple-tank liquid level system. *ISA Transactions* **122**, 146–162 https://doi.org/10. 1016/j.isatra.2021.04.021

Mehndiratta, M., Kayacan, E., Reyhanoglu, M. and Kayacan, E. (2020) Robust tracking control of aerial robots via a simple learning strategy-based feedback linearization. *IEEE Access* **8**, 1653–1669 https://doi.org/10. 1109/ACCESS.2019.2962512

Neto, R.C., Trindade, F.L.A., Marques, B.R.A., Azevedo, G.M.S., Barbosa, E.J. and Barbosa, E.A.O. (2023) An aeropendulum-based didactic platform for the learning of control engineering. *Journal of Control, Automation and Electrical Systems* https://doi.org/10. 1007/s40313-022-00981-4

Nise, N.S. (2019) *Control Systems Engineering*, 8th edn. Wiley, Pomona, CA

Oliveira, L., Bento, A., Leite, V.J.S. and Gomide, F. (2020) Evolving granular feedback linearization: Design, analysis, and applications. *Applied Soft Computing Journal* **86** https://doi.org/10.1016/j.asoc.2019. 105927

Oliveira, L., Bento, A., Leite, V.J.S. and Gomide, F. (2020b) Comparisons of robust methods on feedback linearization through experimental tests. *IFAC-PapersOnLine* **53**, 7983–7988 https://doi.org/10.1016/j.ifacol. 2020.12.2218

Rafiuddin, N. and Khan, Y.U. (2022) Nonlinear controller design for mechatronic aeropendulum. *International Journal of Dynamics and Control* https://doi.org/10.1007/s40435-022-01080-7

Saleem, O., Rizwan, M., Zeb, A.A., Ali, A.H. and Saleem, M.A. (2020) Online adaptive pid tracking control of an aero-pendulum using pso-scaled fuzzy gain adjustment mechanism. *Soft Computing* **24**, 10629–10643 https: //doi.org/10.1007/s00500-019-04568-1

Silva, H.R.M., Ramos, I.T.M., Cardim, R., Assunção, E. and Teixeira, M.C.M. (2020) Identification and switched control of an aeropendulum system. In: *Proceedings of the XXIII Congresso Brasileiro de Automática*. SBA Sociedade Brasileira de Automática, Porto Alegre, Brazil, 1–6. https://www.sba.org.br/open journal systems/index.php /cba/article /view/1429

Slotine, J.-J.E. and Li, W. (1991) *Applied Nonlinear Control*. Prentice Hall, Englewood Cliffs, NJ.

Yamanaka, H.F., Bispo, C.A.S., Breganon, R., Ribeiro, F.S.F., Almeida, J.P.L.S. and Alves, U.N.L.T. (2022) Construção e controle seguidor via lqr de um sistema aeropêndulo. In: *Proceedings of the XXIV Congresso Brasileiro de Automática*. SBA Sociedade Brasileira de Automática, Fortaleza, Brazil, 1–7. https://doi.org/10.20906/CBA2022/3193. In Portuguese

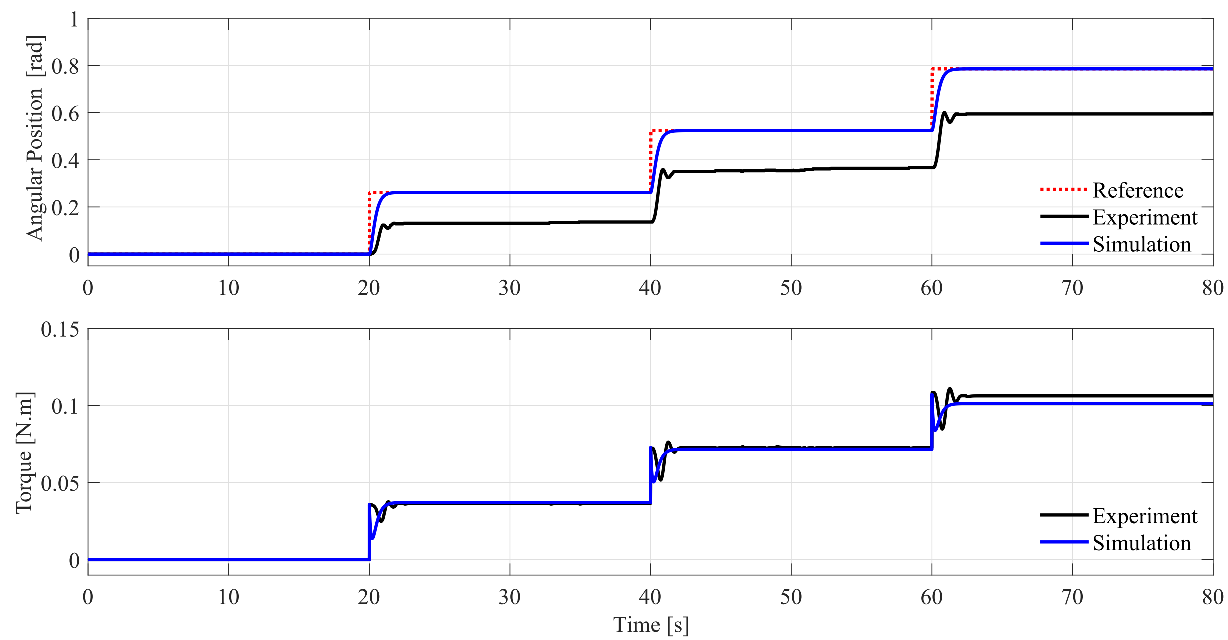

Figure 4. Simulation and experimental result of the feedback linearization (59) controlling the Aeropendulum system using the reference (60)

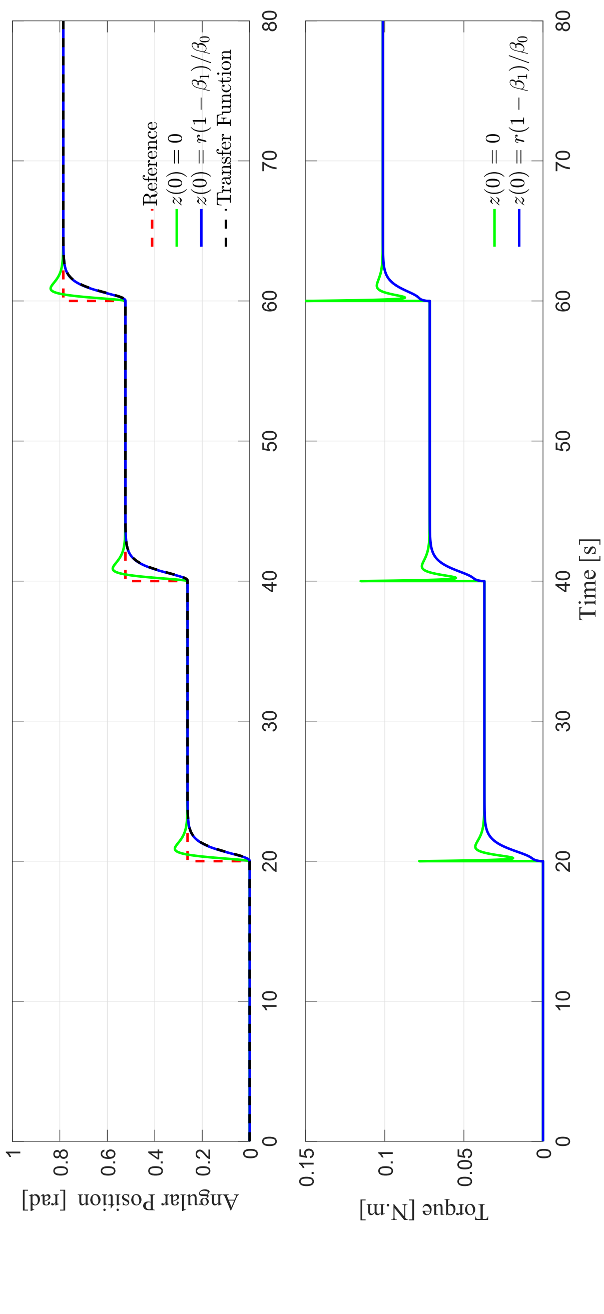

Figure 5. Influence of the use of the initial condition $z(0)$ in the variable $z(t)$ (13) on the integral feedback linearization (61) when controlling the Aeropendulum system using the reference (60)

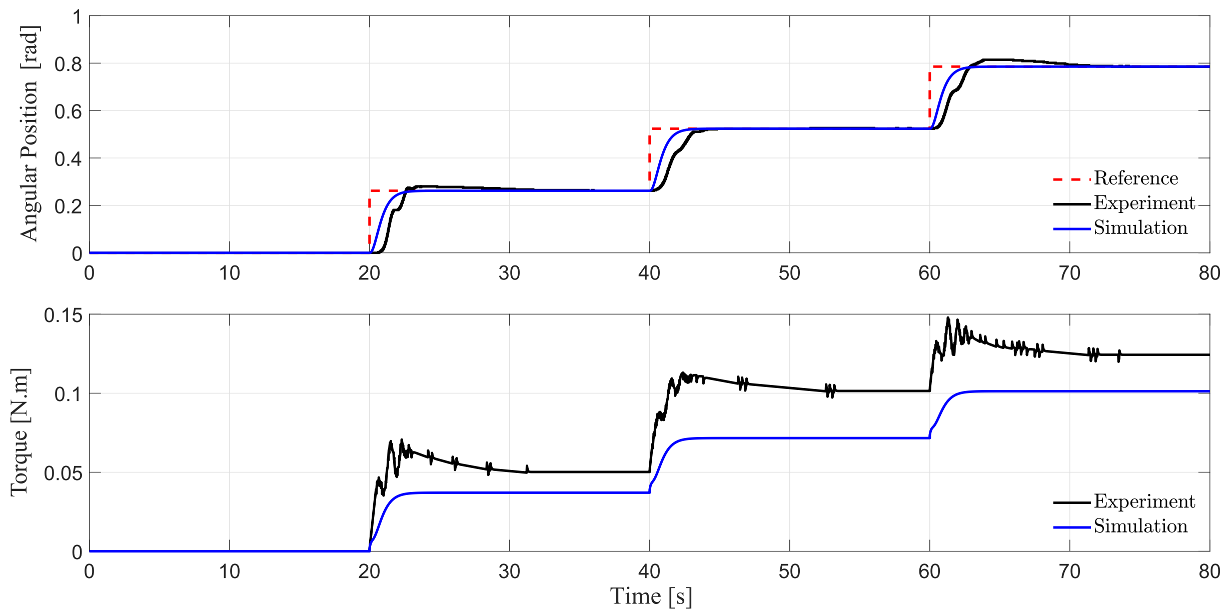

Figure 6. Simulation and experimental result of the integral feedback linearization (61) controlling the Aeropendulum system using the reference (60).

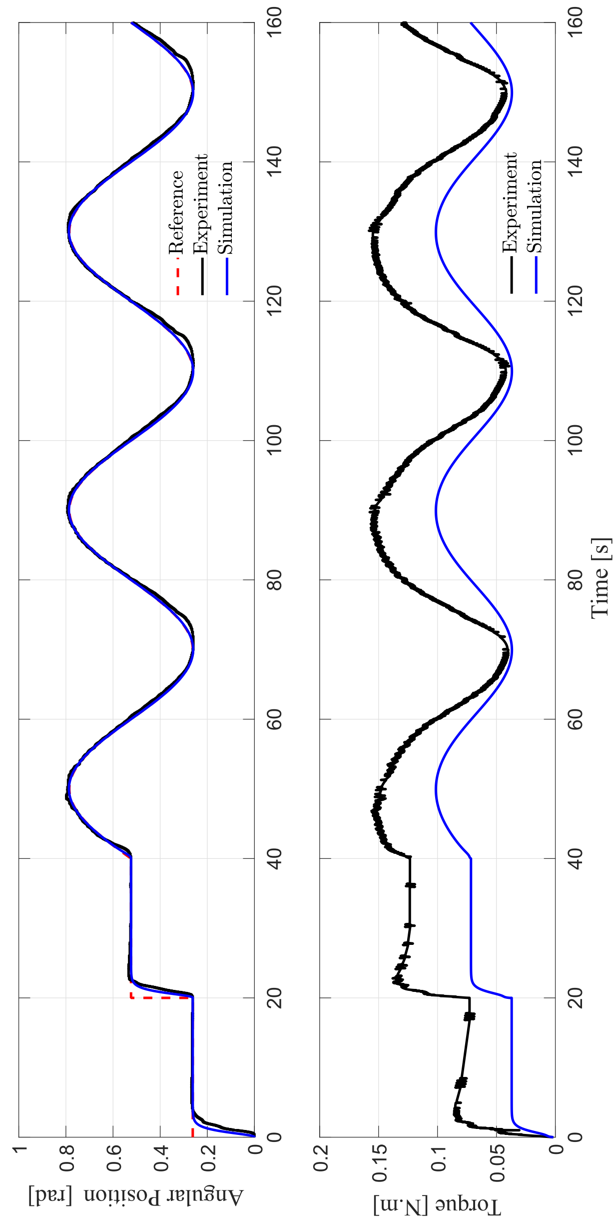

Figure 7. Simulation and experimental result of the integral feedback linearization (61) controlling the Aeropendulum system using the reference (62)